Comparing the inspiral of irrotational and corotational binary neutron stars

Matthew D. Duez[1], Thomas W. Baumgarte[1,2], Stuart L. Shapiro[1,3], Masaru Shibata[4], and Kōji Uryū[5]
[1] *Department of Physics, University of Illinois at Urbana-Champaign, Urbana, IL 61801*
[2] *Department of Physics and Astronomy, Bowdoin College, Brunswick, ME 04011*
[3] *Department of Astronomy & NCSA, University of Illinois at Urbana-Champaign, Urbana, IL 61801*
[4] *Graduate School of Arts and Sciences, University of Tokyo, Komaba, Meguro, Tokyo 153-8902, Japan*
[5] *Department of Physics, University of Wisconsin-Milwaukee, P.O. Box 413, Milwaukee, WI 53201*

We model the adiabatic inspiral of relativistic binary neutron stars in a quasi-equilibrium (QE) approximation, and compute the gravitational wavetrain from the late phase of the inspiral. We compare corotational and irrotational sequences and find a significant difference in the inspiral rate, which is almost entirely caused by differences in the binding energy. We also compare our results with those of a point-mass post-Newtonian calculation. We illustrate how the late inspiral wavetrain computed with our QE numerical scheme can be matched to the subsequent plunge and merger waveform calculated with a fully relativistic hydrodynamics code.

PACS numbers: 04.30.Db, 04.25.Dm, 97.80.Fk

I. INTRODUCTION

Binary neutron stars are among the most promising sources for the detection of gravitational waves by the laser interferometers currently under development, including LIGO, VIRGO, GEO and TAMA (see [1] for the first preliminary data analysis from the TAMA detector). Typical binary neutron stars are expected to complete about 16,000 orbital periods (corresponding to about 15 minutes) while sweeping through LIGO's frequency band between 10 and 1000 Hz [2]. Accurate knowledge of the binary inspiral and the associated gravitational waveform is crucial to enhance our chances of detecting the signal in the noisy output of the laser interferometer.

The evolution of binary neutron stars proceeds in different stages. By far the longest is the initial quasi-equilibrium *inspiral* phase, during which the stars move in nearly circular orbits, while the separation between the stars decreases adiabatically as energy is carried away by gravitational radiation. The quasi-circular orbits become unstable at the innermost stable circular orbit (ISCO), where the inspiraling system enters a *plunge and merger* phase. The merger and coalescence of the stars happens on a dynamical timescale, and produces either a black hole or a larger neutron star, which may collapse to a black hole at a later time. The final stage of the evolution is the *ringdown* phase, during which the merged object settles down to equilibrium.

The early inspiral phase, for large binary separations, can be modeled very accurately with post-Newtonian (PN) methods, e.g. [3]. Recently, the convergence of these PN expansion has been improved by the introduction of Padé approximants [4], and an alternative PN "effective one-body" approach has also been suggested [5] (see also [6] and references therein). It is generally accepted that the plunge and merger phase has to be simulated by means of a self-consistent, fully relativistic hydrodynamics calculation (see [7] for the first such simulation). During the late ringdown phase, the merged object can be approximated as a distorted equilibrium object, so that perturbative techniques can be applied (e.g. [8,9]).

It is likely, however, that PN point-mass techniques break down somewhat outside of the ISCO, when finite-size and relativistic effects become important. It is hard to imagine that fully hydrodynamical numerical calculations will be able to follow the inspiral reliably by beginning far beyond that point, through many orbital periods, all the way to the ISCO, followed by plunge and merger. Such calculations would accumulate significant amounts of numerical error and would be computationally prohibitive. This leaves a gap between the regimes that PN and fully numerical calculations can model. Filling this gap for the late inspiral, immediately prior to plunge, therefore requires an alternative approach (in the case of binary black holes, this problem has been called the "intermediate binary black hole" problem [10]).

We have recently adopted a quasi-equilibrium (QE) approach to model the late inspiral [11]. This approach takes advantage of the fact that during the inspiral phase, the binaries evolve slowly on nearly circular orbits. The matter distribution can therefore be computed independently by assuming the stars to be in quasi-equilibrium (e.g. [12,13]). These pre-determined matter profiles, which satisfy the hydrodynamic equations of quasi-static equilibrium, can then be inserted into Einstein's field equations as source terms and the hydrodynamic equations do not have to be solved again (see the "hydro-without-hydro" approach discussed in [14]). For a given separation, we evolve the binary for about two orbital periods to determine the gravitational wave form and luminosity. We repeat the calculation for a discrete set of separations, which then allows us to construct the entire late inspiral together with its gravitational wave sig-

nal. The QE method is described in more detail in [11] and in Section II A below. We have also tested and calibrated this method for a model problem in relativistic scalar gravitation [15], where the QE wavetrain could be compared with the full wavetrain calculated by an exact numerical integration.

In [11] we presented a prototype calculation for a corotational binary sequence. It is unlikely, however, that binary neutron stars can maintain corotation during inspiral [16]. In this paper, we therefore compare with the more realistic case of irrotational binary neutron stars. By comparing the results we thereby explore the sensitivity of the wavetrain to the internal fluid velocities. We discuss the criterion which determines the point of breakdown of the QE approximation just outside the ISCO. We thus establish the innermost separation at which a QE calculation can provide initial data for future dynamical simulations of the plunge and merger. Finally, we compare our computational results for the late inspiral with a point-mass PN calculation of the same epoch.

The paper is organized as follows. In Section II we describe our numerical methods and resulting waveforms (Section II A), present a first order PN formalism (Section II B), explain the construction of an inspiral wavetrain (Section II C), and finally compare corotational and irrotational sequences, in both the numerical and PN approach (Section II D). In Section III we illustrate how an entire wavetrain, spanning both the late inspiral and the plunge and merger phases, can be constructed by matching QE and fully dynamical results. We briefly summarize our results in Section IV.

II. IRROTATIONAL AND COROTATIONAL BINARY INSPIRAL

A. Numerical results

We adopt a quasi-equilibrium (QE) approximation to study the adiabatic, late inspiral of binary neutron stars, taking advantage of the fact that in this regime the orbital decay timescale is much longer than the orbital period, and, in addition, the gravitational radiation has negligible effect on the structure of the stars (see [11] for details). In this approximation, the inspiral is modeled as a sequence of "snapshots" of binaries in quasi-circular orbit. In this paper we generalize the results of [11] for corotational binaries (based on the models of [12]) to irrotational binaries (based on the models of [13]) and analyze the effect of spin on the inspiral. The snapshots used were constructed under the assumptions that the metric is asymptotically and conformally flat, although the metric ceases to be conformally flat as we evolve it to generate waveforms. These models provide the data to construct binding energy curves, which give the total mass-energy $M(r)$ as a function of separation r for circular binaries of fixed rest (baryonic) mass.

We use these binary models to provide the matter source terms in the Einstein field equations, which we integrate numerically with the formalism and code described in [17] (see also [18]) and used in [11]. For binary separations where the QE approximation is valid, the hydrodynamic equations do not need to be resolved after the initial time . Instead, we freeze the matter variables at their equilibrium values and move the stars on circular orbits while allowing the metric to evolve dynamically. We typically evolve the binary for about two orbital periods for each orbital separation, which is sufficient to read off the gravitational waveform h and the gravitational wave luminosity $-dM/dt$. The initial gravitational wave signal is corrupted by noise contained in the approximate initial data, which quickly propagates off the numerical grid leaving a periodic wave signal from the binary. Repeating the integration for various binary separations r yields $h(r)$ and $dM/dt(r)$ as a function of separation. The inspiral rate can then be found by combining the luminosity with the derivative of the binding energy with respect to separation,

$$\frac{dr}{dt} = \frac{dM/dt}{dM/dr}. \tag{1}$$

Integrating this equation yields the separation r as a function of time t. The gravitational wavetrain $h(t)$ can finally be constructed by using $r(t)$ to fit the discrete waveforms $h(r)$ together in a smooth and continuous fashion. This QE approach has also been tested and calibrated for a model problem in relativistic scalar gravitation ([15]).

Both the corotational and the irrotational sequences terminate at some innermost circular orbit (ICO), at which the quasi-equilibrium approximation breaks down. For the corotational sequences, this ICO corresponds to the innermost stable circular orbit (ISCO) at which the equilibrium orbits become unstable, and at which the plunge and merger of the binary set in. Typical irrotational equilibrium sequences terminate before they reach the ISCO, when they form cusp-like structures at the inner edges of the stars [13,19]. The cusps indicate the onset of mass overflow. The termination of the equilibrium sequence indicates the break-down of the QE approximation, since no equilibrium object exists with this separation. For both the corotational and the irrotational sequences, we denote the mass-energy at the innermost circular orbit as $M_{\rm ICO}$.

By adopting QE matter sources in our evolution calculations, we assume that these remain stationary in a co-rotating frame of reference over an orbital period. As a necessary condition for this to be true, we have to ensure that the binary does not reach the ICO in approximately one orbital period P. Since the energy emitted by the

TABLE I. Irrotational Sequence

z_A [a]	M/M_0 [b]	$\Omega_{\rm orb}M_0$	AM_0 [c]	dM/dt	r/M_0 [d]	dr/dt	$N_{\rm cyc}$ [e]	ξ
0.500	0.95261	0.00587	0.0190	4.94e-09	14.7	2.21e-05	0.0	0.001582
0.474	0.95237	0.00648	0.0219	8.022e-09	13.7	2.79e-05	77.1	0.00250
0.444	0.95210	0.00722	0.0234	1.14e-08	12.7	3.73e-05	144.9	0.00351
0.412	0.95177	0.00808	0.0261	1.78e-08	11.8	5.12e-05	198.3	0.00552
0.375	0.95141	0.00913	0.0290	2.80e-08	10.8	7.37e-05	242.4	0.00898
0.333	0.95100	0.0104	0.0335	4.84e-08	9.89	0.000110	277.0	0.0168
0.286	0.95052	0.0119	0.0379	8.20e-08	8.99	0.000169	302.8	0.0343
0.231	0.95001	0.0138	0.0440	1.47e-07	8.10	0.000277	322.1	0.0896
0.167	0.94949	0.0159	0.0525	2.79e-07	7.28	0.000563	334.9	0.483
$*$ 0.130	0.94929	0.0169	0.0569	3.69e-07	6.91	0.00135	338.5	4.90
$*$ 0.111	0.94926	0.0170	0.0580	3.87e-07	6.78	0.0121	339.1	∞

[a] z_A is defined to be the ratio of the separation between the innermost points and the outermost points on the stars.
[b] M_0 is the total rest mass of the system, i.e., twice the rest mass of an individual star.
[c] A is the amplitude of gravitational waves on the rotation axis.
[d] r is defined as the average of the coordinate distance from the origin of the nearest and farthest points on a neutron star. Thus, it is the coordinate radius of the "center" in $\kappa = 1$ units and the metric and coordinate system of [12,13].
[e] $N_{\rm cyc}$ is the number of gravitational wave cycles from our initial configuration (i.e. that of largest r) to the indicated separation.
$*$ QE approximation is invalid: $\xi > 1$.

TABLE II. Corotational Sequence

z_A	M/M_0	$\Omega_{\rm orb}M_0$	AM_0	dM/dt	r/M_0	dr/dt	$N_{\rm cyc}$	ξ
0.475	0.952098	0.00656	0.0217	8.06e-09	13.7	4.57e-05	0.0	0.00343
0.45	0.95190	0.00715	0.0236	1.13e-08	12.9	3.66e-05	46.6	0.00486
0.400	0.951493	0.00843	0.0270	2.07e-08	11.4	6.40e-05	128.1	0.00938
0.375	0.95131	0.00922	0.0299	3.04e-08	10.8	9.32e-05	152.0	0.01416
0.350	0.951106	0.0102	0.0341	4.82e-08	10.1	0.000130	168.8	0.0236
0.300	0.950752	0.0114	0.0368	7.06e-08	9.27	0.000242	189.8	0.0429
0.275	0.950569	0.0122	0.0393	9.20e-08	8.84	0.000320	196.5	0.0656
0.250	0.950471	0.0130	0.0415	1.16e-07	8.45	0.000422	201.6	0.09014
0.225	0.950329	0.0138	0.0446	1.52e-07	8.09	0.000557	205.5	0.143
0.200	0.950228	0.0146	0.0477	1.93e-07	7.78	0.000744	208.4	0.219
0.175	0.950093	0.0154	0.0500	2.36e-07	7.47	0.00101	210.6	0.393
0.15	0.950031	0.0161	0.0540	3.02e-07	7.21	0.00140	212.2	0.645
0.125	0.950024	0.0168	0.0565	3.59e-07	6.98	0.00204	213.3	0.761
$*$ 0.100	0.949935	0.0174	0.0595	4.31e-07	6.75	0.00312	214.1	1.77

binary per period is $(dM/dt)P$, this condition holds as long as the dimensionless ratio

$$\xi \equiv \frac{|dM/dt|P}{M - M_{\rm ICO}} \tag{2}$$

is less than unity. Identifying the orbital timescale $t_{\rm orb}$ with P and the gravitational wave inspiral timescale $t_{\rm GW}$ with $M/|dM/dt|$ shows that the condition $\xi < 1$ is identical to

$$\frac{M - M_{\rm ICO}}{M} > \frac{t_{\rm orb}}{t_{\rm GW}}. \tag{3}$$

Eq. (3) states that, for infinitesimally small $t_{\rm orb}/t_{\rm GW}$, we can apply the QE approximation arbitrarily close to the ICO. However, if $\xi > 1$, the binaries will overshoot the innermost equilibrium orbit from their current separation in less than one orbital period, causing a breakdown in quasi-equilibrium.

The above criterion is not only useful for determining the limits of the QE approximation, but also for choosing the separation for assigning initial data for dynamical simulations of the plunge and merger. In order to reduce computational resources and accumulation of numerical error, one would like to impose such initial data as close to the ICO as possible. Very close to the ICO, however, the approximations of the QE approach break down, as indicated by Eq. (2). The separation at which $\xi \approx 1$ is therefore a suitable compromise for terminating the QE approach, and imposing initial data for dynamical simulations.

In Tables I and II we summarize our numerical results for irrotational and corotational binaries. For both

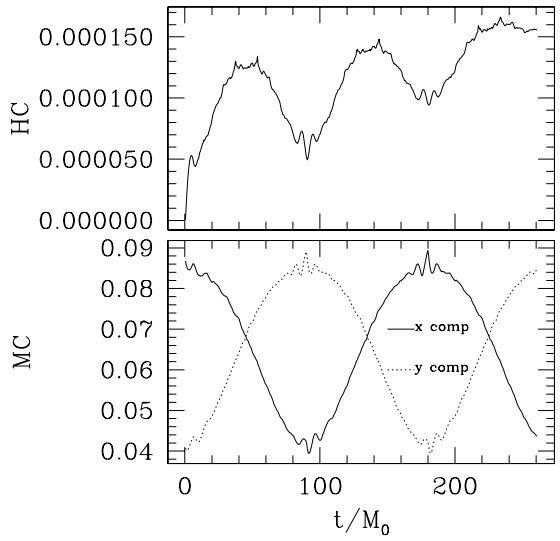

FIG. 1. The L2 norm of the Hamiltonian constraint and of the x and y components of the momentum constraint for corotating binaries with separation parameter $z_A = 0.1$ orbiting about the z-axis. The Hamiltonian constraint is normalized to the initial value of $16\pi M$, the momentum constraint to the L2 norm of the initial value of $8\pi S_x$, where S_x is the dominant component of the initial matter current. The L2 norm is defined as $L2(f) = \sqrt{\sum_i f_i^2}$

cases the stars are modeled as polytropes with pressure $P = \kappa\rho_0^{1+1/n}$, where ρ_0 is the rest-mass density, n is the polytropic index, and κ is a constant. We set $n = 1$ and non-dimensionalize our results by setting $\kappa = G = c = 1$. In these units, the individual stars have a rest mass $m_0 = 0.1$, which is about 55% of the maximum allowed rest mass of isolated, spherical nonrotating stars, and corresponds to a compaction of $m_\infty/R_\infty = 0.088$ in isolation. Here m_∞ and R_∞ are the mass-energy and areal radius (i.e. radius defined by the area of a constant-r shell) of the individual (spherical) stars at infinite binary separation. Our results apply to arbitrary mass stars with this compaction and equation of state. For both cases, we study models up to and past $\xi = 1$. In Figure 1, we verify that our evolution code satisfies the Hamiltonian and momentum constraints. This is a nontrivial test of our method: The matter profiles are determined by solving the constraint equations in the QE approximation. The fact that they remain satisfied during the field evolution demonstrates that the spacetime remains close to quasi-equilibrium, even as gravitational radiation is generated and the metric is determined dynamically.

B. Post-Newtonian treatment

We adopt the formalism developed in [20] to study the binary inspiral in a first order PN approximation (note that PN techniques have been extended to at least third order; see, e.g. [6]). In particular, we consider a system of two point masses in circular orbit with binary separation r, total orbital angular momentum $\mathbf{L_N}$, and total spin angular momentum $\mathbf{S}$. In isolation, each point mass has a mass-energy m_∞. From [20] we then find the orbital frequency

$$\Omega_{\rm orb}^2 = \frac{\mu}{r^3}\big(1 - \frac{11}{4}\frac{\mu}{r} - \frac{5}{\mu r^2}\mathbf{L_N}\cdot\mathbf{S}\big), \tag{4}$$

the total mass-energy

$$M = \mu + \frac{\mu}{4}\big(-\frac{1}{2}\frac{\mu}{r} + \frac{27}{32}\big(\frac{\mu}{r}\big)^2 - \frac{3}{2r^2}\mathbf{L_N}\cdot\mathbf{S}\big), \tag{5}$$

and the luminosity

$$\frac{dM}{dt} = -\frac{2}{5}\big(\frac{\mu}{r}\big)^5\big(1 - \frac{379}{42}\frac{\mu}{r} + 4\pi\big(\frac{\mu}{r}\big)^{3/2} - \frac{37}{3}\big(\frac{\mu}{r}\big)^{3/2}\mathbf{L_N}\cdot\mathbf{S}\big). \tag{6}$$

Here we identify

$$\mu = \begin{cases} 2m_\infty & \text{irrotational} \\ 2(m_\infty + \frac{1}{2}I\Omega_{\rm orb}^2) & \text{corotational} \end{cases} \tag{7}$$

for the total mass-energy of each star in isolation. To compare with the binaries of Section II A, we choose

$$\mathbf{L_N} = r^2\Omega_{\rm orb}\mathbf{e_z} \tag{8}$$

for the total orbital angular momentum and

$$\mathbf{S} = \begin{cases} \mathbf{0} & \text{irrotational} \\ 2I\Omega_{\rm orb}\mathbf{e_z} & \text{corotational} \end{cases} \tag{9}$$

for the spin angular momentum.

In the above, r is the separation of the point masses in harmonic coordinates, and the moment of inertia of each mass, I, is calculated for a slowly rotating (nearly TOV) relativistic star [21]. Note that, for the corotational case, μ, and $\Omega_{\rm orb}$ must be solved simultaneously to PN order.

C. Constructing Wavetrains

We extract gravitational wave data from our QE simulations by matching the numerical data near the boundaries of our grids to the $l = 2$, $m = \pm 2$ Moncrief [22] variables R_{22+} and R_{22-} (see Appendix A for details). From these, the energy luminosity is given by

$$\frac{dM}{dt} = \frac{r^2}{32\pi}\big[(\partial_{\rm t}R_{22+})^2 + (\partial_{\rm t}R_{22-})^2\big]. \tag{10}$$

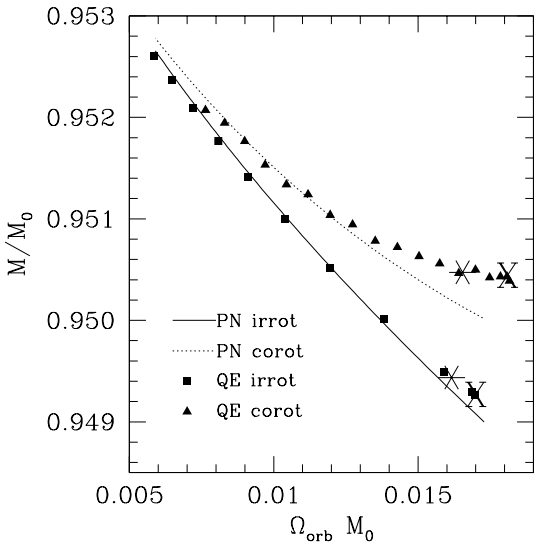

FIG. 2. The total mass-energy M as a function of orbital frequency for corotational and irrotational models. The cross marks the ISO, the asterisk the location at which $\xi = 1$.

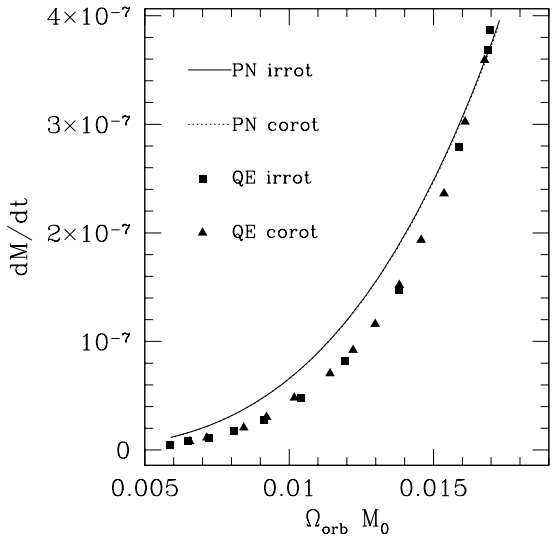

FIG. 3. The gravitational wave luminosity dM/dt as a function of orbital frequency for corotational and irrotational models. The solid and dotted curves nearly coincide.

To generate the wavetrain, we also need to determine the wave amplitude. Both the QE and PN models provide more information than just the quadrupole amplitudes, but we have found [11] that the amplitudes of other modes are much smaller than the $l = 2$, $m = \pm 2$ modes, and we ignore them below. The asymptotic amplitudes of h_+ and $h_\times$ for these modes are identical along the axis of rotation, and are called A below. This amplitude is related to the luminosity by the quadrupole relation

$$A = \frac{1}{\Omega_{\rm GW}} \sqrt{10 \frac{dM}{dt}}, \tag{11}$$

where $\Omega_{\rm GW} = 2\Omega_{\rm orb}$ is the frequency of the waves. This gives $A(r)$, which can be converted to $A(t)$ by solving Eq. (1). Then the complete wavetrain as seen by an observer on the rotation axis at a distance r_s from the source is given by

$$r_s h(t) = A(t) \cos\left(\int_0^t \Omega_{\rm GW}(t')dt'\right) \tag{12}$$

D. Comparing irrotational and corotational inspiral

In Figure 2, we show the total mass-energy M of irrotational and corotational inspiral sequences (along which the total rest mass M_0 is conserved). We parameterize the binary separation by $\Omega_{\rm orb}$, the orbital angular frequency as measured by a distant observer, since it is an invariant. Note that infinite separation corresponds to $\Omega_{\rm orb} = 0$. The PN and QE results agree quite well

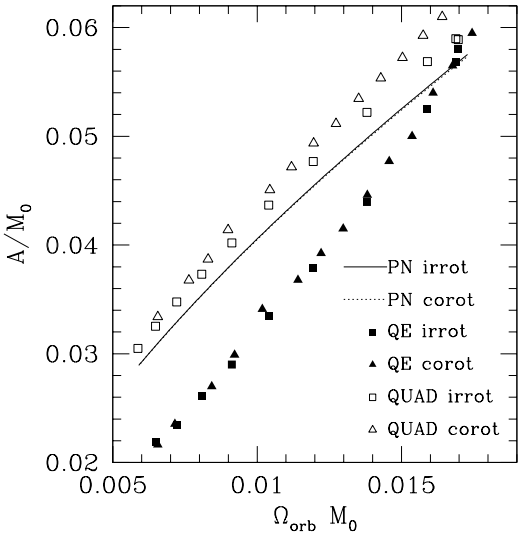

FIG. 4. Gravitational wave amplitude along the axis of rotation in the QE, PN and Newtonian quadrupole approximation. The PN curves for the two cases, which are based on Eq. (11), are hardly distinguishable.

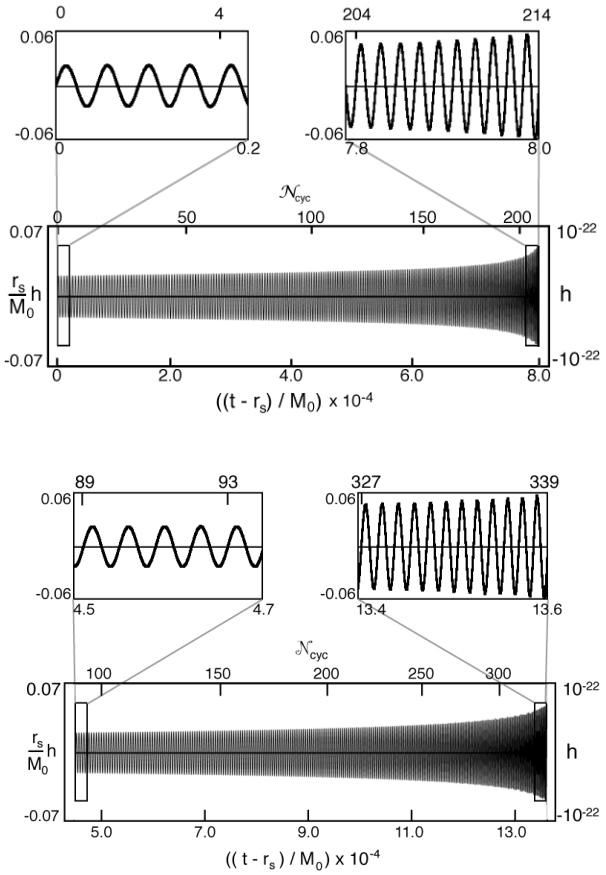

FIG. 5. The final two hundred cycles of the inspiral waveform for corotating (top) and irrotating (bottom) binaries.

for large separations, while for small separations we find growing deviations between the two approaches. This is not surprising, since at small separations both tidal interactions and relativistic effects play an increasingly important role. Finite size effects are not taken into account by the point-mass calculation of the PN approach. The inclusion of 2 and 3PN terms will not improve the agreement substantially, due to the dominance of finite size effects [23,24]. For small separations, the mass-energy, and hence the binding energy, of irrotational and corotational sequences is quite different. This effect is due to the extra spin rotational energy of the corotating binaries, which causes their total energy to be larger than that of the irrotational binaries. As we will see below, this change in M, and hence dM/dr, dominates the difference in the inspiral rate dr/dt.

In Figure 3, we plot dM/dt for each model. Note that the gravitational wave luminosity dM/dt is very similar for the irrotational and corotational sequence in either the QE or the PN approximation. In Figure 4, we show the gravitational wave amplitudes as measured along the axis of rotation and compare two different numerical results with the PN values. From our numerical binary models, we predict the gravitational wave amplitude, both from the Newtonian quadrupole approximation, where the quadrupole moments are computed by numerical quadrature of the density and velocity fields, and by dynamically evolving the (relativistic) gravitational fields and reading off the wave amplitudes on the outer edge of the numerical grid, as described in section IIC.

For large separations, the quadrupole and PN results agree quite well, while the QE results differ by $\sim 30\%$. We attribute this difference to the inaccurate boundary treatment in our dynamical evolution (see [11]). Gravitational radiation can only be read off accurately in the far (wave) zone, at separations greater than a gravitational wavelength $\lambda_{\rm GW}$. In our simulations, however, we are restricted to numerical grids which only extend to a fraction of a gravitational wavelength, $r_{\rm max} \sim 0.1-0.35\lambda_{\rm GW}$. For large binary separations, the frequency $\Omega_{\rm GW}$ is small, and hence $\lambda_{\rm GW}$ is large. For fixed outer boundary $r_{\rm max}$ this implies that $r_{\rm max}/\lambda_{\rm GW}$ is smaller for larger binary separations, causing a more inaccurate wave extraction. As the separation becomes smaller, the QE and quadrupole results agree increasingly well. Simultaneously we expect the PN point-mass treatment to become increasingly inaccurate for small separations, since it neglects finite size effects. This trend is reflected in the growing deviations between the PN and quadrupole results in Figure 4.

The differences between the irrotational and corotational wave amplitudes are very small in all three approaches. This is quite intuitive, since the gravitational wave emission is dominated by the matter density distribution, which is fairly similar for the two sequences, while matter current distributions play a less important role. The poor handling of the outer boundaries in the QE approximation affects both sequences in the same systematic way, which allows us to make a meaningful comparison.

The findings of this comparison with regard to the inspiral rate can be anticipated from Eq. (1). The numerator on the right hand side, dM/dt is very similar for irrotational and corotational sequences, while the denominator, dM/dr is different. The latter therefore causes the inspiral rate $|dr/dt|$ to be smaller for irrotational than for corotational binaries. This effect can be understood very easily even by a crude Newtonian argument, where the total mass-energy of the star can be written as a sum

$$M \sim M_0 - \frac{M_0^2}{2r}\ \left[+2\frac{1}{2}I\Omega^2\right] \sim M_0 - \frac{M_0^2}{2r}\ \left[+I\frac{M_0}{r^3}\right]. \tag{13}$$

In Eq. (13), the first term on the right-hand side is the energy of a spherical polytrope (rest + internal + gravitational potential energy), the second term is the combined orbital kinetic and gravitational potential energy

for circular equilibrium, and the third term, in square brackets, denotes the spin kinetic energy. Note that the term in the square brackets applies only to the corotational sequence. For a given separation, the energy of a corotational binary is thus larger than that of an irrotational binary by the spin energy of the individual stars. Taking a derivative with respect to r yields

$$\frac{dM^{\rm corot}}{dr} \sim \frac{dM^{\rm irrot}}{dr} - 3I\frac{M_0}{r^4}. \qquad (14)$$

Inserting this into Eq. (1), and using the result that dM/dt is nearly identical for both sequences, immediately shows that

$$\left|\frac{dr}{dt}\right|_{\rm corot} > \left|\frac{dr}{dt}\right|_{\rm irrot}. \qquad (15)$$

Correspondingly, the frequency of the gravitational wave train increases at a faster rate for corotational binaries, which we illustrate in Figure 5.

III. COMPUTING THE FULL WAVETRAIN THROUGH COALESCENCE

As we have argued in Section II A, the QE approach could provide accurate numerical initial data for fully relativistic hydrodynamics simulations of the plunge and merger at a separation for which $\xi \gtrsim 1$. Starting at this separation guarantees that the binary reaches the dynamical instability at the ICO within about one orbital period. This approach provide intrinsically more accurate initial data than those imposed at the ICO (where the QE approximation breaks down). Moreover, the QE approach allows noise contained in the initial data to be radiated away, thereby producing more accurate equilibrium data. In the QE approach, the initial noise can be easily distinguished from the later periodic binary signal, whereas in a dynamical plunge simulation it may be more difficult to distinguish the propagation of initial noise from the intrinsically short-lived coalescence waveform.

In Figure 6, we provide an illustration of what the combined late inspiral-plunge wavetrain might look like. We compute the late inspiral wavetrain using the QE method for an irrotational binary sequence with stars of rest mass $m_0 = 0.146$, which corresponds to 81% of the maximum allowed rest mass of an isolated, nonrotating star, and to a compaction of m_∞/R_∞ =0.14 in isolation [25]. We then match this to the full hydro dynamical waveform for the plunge and merger of this same binary as computed by Shibata and Uryū [7,27]. In order to get a continuous waveform, we adopt the same wave extraction rules as in [7], namely, $h_\times$ is read off the rotation axis at the edge of the numerical grid, located at $r = 0.35\lambda_{\rm GW}$. The continuous wavetrain is constructed in the following manner:

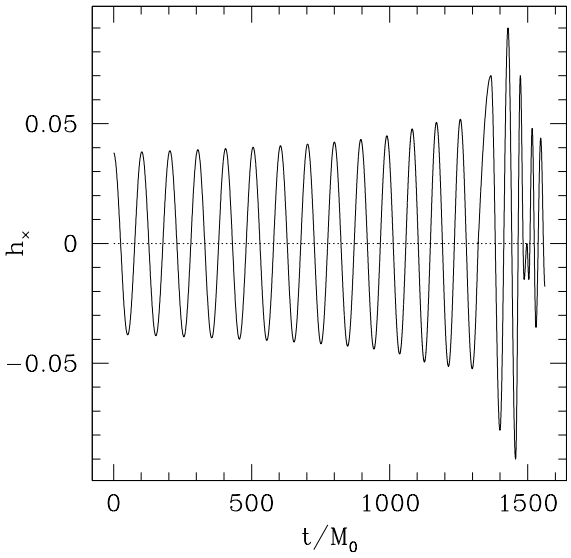

FIG. 6. A match of the total late QE inspiral wavetrain to the plunge and merger waveform, both constructed from numerical simulations in general relativity. Here we connect the last 13 orbits of the inspiral, computed in the QE approximation, to the plunge calculation of [7]. The ICO is reached at t/M_0 =1330, around which point we pass from the adiabatic inspiral to the plunge and merger phase. Here $h_\times = \frac{r_s}{M_0}\tilde{\gamma}_{\rm xy}$, where r_s is the distance from the source and $\tilde{\gamma}_{ij}$ is the conformal 3-metric on the rotation axis. This coalescence scenario leads to merger and immediate black hole formation. For $M_0 = 2 \times 1.5 M_\odot$ and r_s =100 Mpc, the maximum amplitude of the metric perturbation is $\sim 5 \times 10^{-21}$.

From $t = 0$ to $t = 1321M_0$ at the ICO, we use QE data. A smooth (sine) function with the appropriate gravitational wave frequency and amplitude is used to match the QE data to the plunge data. The raw plunge data given in [7] begins at $t = 1367M_0$.

The location and nature of the transition from quasi-periodic inspiral to rapid plunge is of great astrophysical interest because it is sensitive to details of the binary neutron star system, in particular the equation of state and rotation rate [28]. As illustrated above, the QE method, in conjunction with a relativistic hydrodynamics code, could allow one to obtain the complete wavetrain from late inspiral through plunge and merger, and at a very reasonable computational cost.

IV. SUMMARY

We study the late inspiral of binary neutron stars and, by comparing corotational and irrotational sequences, explore the effect of internal fluid motions on the inspiral rate. We find the gravitational wave luminosity is very similar for any given radius. However, the inspiral of

corotational binaries proceeds faster.

We also compare our numerical QE results with a first-order PN calculation. For large binary separations, the poor outer boundary conditions in the numerical calculations introduce significant deviations, while for small separations finite-size effects, which are not taken into account in the PN calculations, can no longer be neglected. Future improvements in wave extraction and outer boundary conditions (see, e.g. [29]) should reduce the discrepancy. These improvements remain a long-term goal for numerical simulations of binary inspiral.

Lastly, we illustrate how QE and fully dynamical results could be matched to produce the entire gravitational wavetrain, covering the late inspiral through the plunge and merger phases. We emphasize that this paper presents only a prototype calculation showing how, in principle, the continuous wavetrain can be assembled from numerical simulations.

ACKNOWLEDGMENTS

We would like to thank REU students J. Mehl, H. Agarwal, P. McGrath, and D. Webber for assistance on Figure 5. TWB gratefully acknowledges financial support through a Fortner Fellowship at the University of Illinois at Urbana-Champaign (UIUC). Much of the calculation and visualization were performed at the National Center for Supercomputing Applications at UIUC. This paper was supported in part by NSF Grant PHY 99-02833 and NASA Grant NAG 5-10781 at UIUC and by NSF Grant PHY00-71044 at the University of Wisconsin.

APPENDIX A: GRAVITATIONAL WAVE EXTRACTION

The two gravitational wave polarizations can be expressed as

$$\begin{aligned} h_+ &= \frac{r}{2}(\gamma^{TT}_{\hat\theta\hat\theta} - \gamma^{TT}_{\hat\phi\hat\phi}) \\ h_\times &= r\gamma^{TT}_{\hat\theta\hat\phi}, \end{aligned} \tag{A1}$$

where the superscript TT denotes transverse-traceless projection, and $\gamma_{\hat{\imath}\hat{\jmath}}$ is the spatial metric in orthonormal spherical-polar coordinates. Note that the amplitudes of h_+ and $h_\times$ are independent of r at large r. We determine h_+ and $h_\times$ from the Moncrief [22] variables G_{lm}, h_{1lm}, H_{2lm} and K_{lm}, which we compute by quadratures of our metric over a spherical shell near the edge of our grid (see [30]). From these we find the gauge-invariant linear combinations $R^{\rm E}_{lm}$. In our code, we work with real, orthonormal combinations of spherical harmonics, and so we compute the amplitudes R_{22+}, which is associated with the mode having angular dependence $(Y_{22}+Y_{2-2})/\sqrt{2}$, and R_{22-}, which is associated with the mode having angular dependence $(Y_{22}-Y_{2-2})/i\sqrt{2}$.

As argued in [30], our gauge conditions approach the TT gauge as r becomes large. In this gauge, the two gravitational wave polarizations can be constructed from

$$h_+ = r\sum_{lm} G_{lm}W_{lm} \qquad h_\times = r\sum_{lm} G_{lm}X_{lm}/\sin\theta. \tag{A2}$$

The Moncrief functions only depend on r and t, while the angular dependence is contained in the W_{lm} and X_{lm}. In the TT gauge, all Moncrief variables vanish except for the G_{lm}, so that the linear combination for the $R^{\rm E}_{lm}$ reduces to

$$R^{\rm E}_{2\pm2} = 2\sqrt{12}\,G_{2\pm2} \tag{A3}$$

for the dominant modes $l=2$, $m=\pm2$. Inserting these into eq. (A2) we then construct

$$\begin{aligned} h_+ &= \frac{r}{2}\sqrt{\frac{5}{16\pi}}(1+\cos^2\theta)(\cos(2\phi)R_{22+} + \sin(2\phi)R_{22-}) \\ h_\times &= r\sqrt{\frac{5}{16\pi}}\cos\theta(-\sin(2\phi)R_{22+} + \cos(2\phi)R_{22-}) \end{aligned} \tag{A4}$$

up to an arbitrary phase. Finally, the amplitude A on the z-axis (i.e. $\theta=0$) is given by

$$A = r\sqrt{\frac{5}{16\pi}}\sqrt{(R_{22+})^2+(R_{22-})^2}. \tag{A5}$$

As a check of the above, one can, by making explicit the time dependence in (A4) ($\phi \to \phi - \Omega_{\rm orb}t$), use Eq. (10) to derive the luminosity-amplitude relationship for quadrupole (e.g. point mass) systems, Eq. (11). The amplitude of the waveform $h(t)$ in Eq. (12) is then equal to $A(t)/r$. (The $1/r$ falloff is restored.)

[1] H. Tagoshi *et.al.*, Phys. Rev. D **63**, 062001 (2001).
[2] K. S. Thorne, in *Black Holes and Relativistic Stars*, edited by R.M. Wald (U. of Chicago Press, Chicago, 1998), p. 59.
[3] L. Blanchet, T. Damour, B.R. Iyer, C.M. Will, and A.G. Wiseman, Phys. Rev. Lett **74** 3515 (1995).
[4] T. Damour, B. R. Iyer, and B. S. Sathyaprakash, Phys. Rev. D **57**, 885 (1998).
[5] A. Buonanno, and T. Damour, Phys. Rev. D **59**, 084006 (1999).
[6] T. Damour, P. Jaranowski and G. Schäfer, Phys. Rev. D **62**, 084011 (2000).
[7] M. Shibata and K. Uryū, Phys. Rev. D **61**, 064001 (2000).
[8] R. H. Price, J. Pullin, Phys. Rev. Lett. **72**, 3297 (1994).

[9] G. Khanna *et. al.*, Phys. Rev. Lett. **83**, 3581 (1999).
[10] P. R. Brady, J. D. E. Creighton, and K. S. Thorne, Phys. Rev. D **58**, 061501 (1998).
[11] M. D. Duez, T. W. Baumgarte, and S. L. Shapiro, Phys. Rev. D **63**, 084030 (2001).
[12] T. W. Baumgarte, G. B. Cook, M. A. Scheel, S. L. Shapiro and S. A. Teukolsky, Phys. Rev. Lett. **79**, 1182 (1997); Phys. Rev. D **57**, 7299 (1998).
[13] K. Uryū and Y. Eriguchi, Phys. Rev. D **61**, 124023 (2000).
[14] T. W. Baumgarte, S. A. Hughes, and S. L. Shapiro, Phys. Rev. D **60**, 087501 (1999).
[15] H.-J. Yo, T. W. Baumgarte and S. L. Shapiro, Phys. Rev. D. **63**, 064035 (2001).
[16] C. S. Kochanek, Astrophys. J. **398** 234 (1992); L. Bildsten and C. Cutler, Astrophys. J. **400**, 175 (1992).
[17] T. W. Baumgarte and S. L. Shapiro, Phys. Rev. D **59**, 024007 (1999).
[18] M. Shibata and T. Nakamura, Phys. Rev. D **52**, 5428 (1995).
[19] K. Uryū, M. Shibata, and Y. Eriguchi, Phys. Rev. D **62** 104015 (2000).
[20] C. M. Will, in *Relativistic Cosmology*, edited by M. Sasaki (Universal Academy Press,1994), p. 95.
[21] W. D. Arnett and R. L. Bowers, Astrophys. J. Suppl. **33**, 415 (1977).
[22] V. Moncrief, Ann. Phys. **88**, 323 (1974).
[23] D. Lai, F. A. Rasio, and S. L. Shapiro, Astrophys. J. **420**, 811 (1994).
[24] T. W. Baumgarte, to appear in Astrophysical Sources of Gravitational Radiation, edited by J. M. Centrella, AIP Conference Proceedings, New York (2001) (also gr-qc/0101045).
[25] Setting the maximum rest-mass of an isolated neutron star equal to about 1.9 $M_\odot$ [26] implies that the stars in our simulations have rest masses of about 1.5 $M_\odot$.
[26] A. Akmal, V. R. Pandharipande, and D. G. Ravenhall, Phys. Rev. C. **58**, 1804-1828 (1998).
[27] In generating the merger waveform in [7], only approximate QE initial data was used. This induces some inaccuracy in the merger phase of the waveform shown in Figure 6. Accordingly, Figure 6 should not be regarded as definitive but, rather, illustrative of the technique and the general shape of the expected waveform.
[28] C. Cutler, T. A. Apostolatos, L. Bildsten, L. S. Finn, E. E. Flanagan, D. Kennefick, D. M. Markovic, A. Ori, E. Poisson, G. J. Sussman, and K. S. Thorne, Phys. Rev. Lett. **70**, 2984 (1993).
[29] N. T. Bishop, R. Gomez, P. R. Holvorcem, R. A. Matzner, P. Papadopoulos and J. Winicour, J. Comp. Phys. **136**, 140 (1997); A. M. Abrahams *et.al.* (The Binary Black Hole Grand Challenge Alliance) Phys. Rev. Lett. **80**, 1812 (1998).
[30] M. Shibata, Prog. Theor. Phys. **101**, 1199 (1999).